

One loop renormalisation of Lattice NRQCD currents for semileptonic $B \rightarrow D^{(*)}$ decays to order $\frac{\bar{p}}{M}$

Peter Boyle
Christine Davies

Department of Physics and Astronomy, University of Glasgow, Glasgow G12 8QQ, UK

UKQCD Collaboration

We present the results of a perturbative calculation to match the axial and vector currents for semileptonic $B \rightarrow D^{(*)}$ decays in lattice NRQCD to the continuum \overline{MS} scheme. The matching is performed to $O(\alpha_s \frac{\bar{p}}{M})$ in Feynman gauge and in the on-shell renormalisation scheme.

The spatial and temporal components of the currents renormalise differently; to this order the matching involves a straightforward renormalisation for the V_0 and A_k currents, and a rank two and four mixing matrix for the A_0 and V_k currents respectively. The resultant one loop corrections are of $O(5\%)$, boding well for the accuracy of forthcoming simulations.

I. INTRODUCTION

Forthcoming B physics experiments such as BaBar, Belle, CLEO III and LHC-b will greatly improve the accuracy with which we know the rates of different decay modes of the B meson, allowing improved determinations of the CKM matrix elements involving the b quark. The exclusive decay $\bar{B} \rightarrow D l \bar{\nu}$ gives access to V_{cb} . For example, at BaBar [1] the decay amplitude at zero recoil will be determined with a statistical error of less than 2% and with similar level of systematic errors, a factor of three improvement over CLEO and LEP data. In order to extract V_{cb} we must divide out the form factor at zero recoil, introducing associated theoretical uncertainties. The form factors for $B \rightarrow D$ decays are calculable within lattice QCD¹, and it will be highly challenging for the community to produce model independent predictions of the form factors with sufficient statistical and systematic precision that theoretical uncertainty matches the improved experimental data.

The decay amplitudes can be factorised into hadronic form factors and perturbative electroweak terms as follows:

$$M(B \rightarrow D^{(*)} l^- \bar{\nu}) = -\frac{iG_F}{\sqrt{2}} V_{cb} \bar{u}_l \gamma_\mu (1 - \gamma_5) v_\nu H^{\mu^{(*)}}, \quad (1)$$

where

$$H^\mu = \langle D(p') | V^\mu | B(p) \rangle = f_+(q^2)(p + p')^\mu + f_-(q^2)(p - p')^\mu, \quad (2)$$

$$H^{\mu^*} = \langle D^*(p', \epsilon) | V^\mu - A^\mu | B(p) \rangle = \left\{ \begin{array}{l} \frac{2i\epsilon^{\mu\nu\alpha\beta}}{M_B + M_{D^*}} \epsilon_\nu^* p'_\alpha p_\beta V(q^2) \\ -(M_B + M_{D^*}) \epsilon^{*\mu} A_1(q^2) \\ + \frac{\epsilon^{*q}}{M_B + M_{D^*}} (p + p')^\mu A_2(q^2) \end{array} \right\}. \quad (3)$$

These are often reparametrised in terms of form factors in the heavy quark effective theory,

$$\langle D(p') | V^\mu | B(p) \rangle = \sqrt{M_B M_D} \{ h_+(v \cdot v')(v + v')^\mu + h_-(v \cdot v')(v - v')^\mu \} \quad (4)$$

$$\langle D^*(p', \epsilon) | V^\mu - A^\mu | B(p) \rangle = \sqrt{M_B M_{D^*}} \left\{ \begin{array}{l} i\epsilon^{\mu\nu\alpha\beta} \epsilon_\nu^* v'_\alpha v_\beta h_V(v \cdot v') \\ -\epsilon^{*\mu}(v \cdot v' + 1) h_{A_1}(v \cdot v') \\ + \epsilon^* \cdot v v^\mu h_{A_2}(v \cdot v') \\ + \epsilon^* \cdot v v'^\mu h_{A_3}(v \cdot v') \end{array} \right\} \quad (5)$$

The weak (vector and axial) currents in a lattice-regulated theory differ from the continuum \overline{MS} currents via their different ultra-violet cut-offs. A correction between the results in the two regularisation schemes is therefore required in order to use simulated lattice hadronic currents in the

¹ There are a number of recent reviews of the status of lattice calculations [2]

more commonly quoted continuum \overline{MS} scheme. Lattice QCD and \overline{MS} have the same infra-red behaviour, so that these correction factors should be dominated by the differing ultra-violet behaviour and one expects that these corrections are calculable within perturbation theory. Knowledge of these renormalisation constants enables the various elements of the Cabibbo-Kobayashi-Maskawa weak mixing matrix to be probed using experimental decay rates and lattice calculations of hadronic matrix elements in conjunction with standard electroweak perturbation theory.

This paper aims to make possible the accurate determination of $B \rightarrow D$ matrix elements by showing how to construct the \overline{MS} currents when using the $O(\frac{1}{M})$ lattice NRQCD action to simulate both the b and c quarks. We perturbatively match the corrections to the weak currents between on-shell quark states in lattice NRQCD to the same current in continuum \overline{MS} with fully relativistic quarks, working consistently to $O(\frac{1}{M})$ throughout. The paper will be constructed as follows: in Section II we will present the one loop correction to the continuum current evaluated between an incoming b quark and outgoing c quark, retaining all terms to order $\frac{\vec{p}}{M}$. This is matched to continuum Euclidean NRQCD to $O(\frac{1}{M})$, giving a basis of continuum NRQCD operators for each of the currents V_0, V_k, A_0, A_k . In Section III we select a basis of operators in the Lattice theory and define the one-loop mixing matrix, giving the projection of each element of a basis for a given Lattice current at one loop on the basis of continuum NRQCD operators. Finally, we use these results to construct relativistic \overline{MS} currents to this order from lattice operators in Section IV.

II. CONTINUUM CALCULATION

We require the continuum renormalisation of the Vector and Axial currents involving an incoming b quark with momentum p and outgoing c quark with momentum p' , i.e. $\bar{u}_c(p')\Gamma u_b(p)$, where either $\Gamma = \gamma_\mu$ or $\Gamma = \gamma_\mu\gamma_5$. At one loop the graphs in Figures 1 to 3 contribute. The calculation was performed in Minkowski space using dimensional regularisation in Feynman gauge, the on-shell \overline{MS} scheme, and having introduced a fictitious gluon mass λ to regulate infra-red divergences. The treatment allowed for non-zero external momenta, keeping terms linear in $\frac{\vec{p}}{M}$ and $\frac{\vec{p}'}{M}$.

In general, we write the perturbative expansion of some quantity, Q , as

$$Q = \sum_{k=0}^{\infty} Q^{[k]} \alpha_s^k. \quad (6)$$

We write the Feynman graph in Figure 1 as $\alpha_s \Lambda^{\Gamma^{[1]}}$ and the leg corrections in Figures 2 and 3 as $\frac{1}{2}\alpha_s \Gamma Z_{\psi_b}^{[1]}$ and $\frac{1}{2}\alpha_s \Gamma Z_{\psi_c}^{[1]}$ respectively. Dropping the external spinors, the total current correction may be written as

$$\Delta\Gamma = \alpha_s \left[\Lambda^{\Gamma^{[1]}} + \frac{1}{2}\Gamma Z_{\psi_c}^{[1]} + \frac{1}{2}Z_{\psi_b}^{[1]} \right], \quad (7)$$

Here both $\Lambda^{\Gamma^{[1]}}$, and Z_ψ contain (cancelling) infra-red divergences of modulus $\frac{\alpha_s}{3\pi} 4 \log \frac{\lambda}{M}$. The result is IR-finite, and we obtain that the \overline{MS} current to one loop and $O(\frac{\vec{p}}{M})$ is as follows ²

$$\Delta\Gamma \cdot \tilde{\Gamma} = C_1 \gamma^\mu + C_2 \frac{p^\mu}{m_b} + C_3 \frac{p'^\mu}{m_c} \quad (8)$$

where,

$$C_1 = \frac{\alpha_s}{3\pi} \left[-3 \frac{1+\xi}{1-\xi} \log \xi + 2\mathcal{C} - 6 \right] \quad (9)$$

$$C_2 = \frac{\alpha_s}{3\pi} \left[-\frac{4}{(1-\xi)^2} + 2\xi \log \xi \frac{\xi-3}{(1-\xi)^3} + \mathcal{C} \left\{ 2 \frac{1+\xi}{(1-\xi)^2} + \frac{4\xi \log \xi}{(1-\xi)^3} \right\} \right] \quad (10)$$

$$C_3 = \frac{\alpha_s}{3\pi} \left[2\xi \frac{1+\xi}{(1-\xi)^2} + 4\xi^2 \frac{\log \xi}{(1-\xi)^3} + \mathcal{C} \left\{ -\frac{4\xi^2}{(1-\xi)^2} + 2\xi \log \xi \frac{1-3\xi}{(1-\xi)^3} \right\} \right] \quad (11)$$

and

² It is worth noting here that at higher orders in the $\frac{\vec{p}}{M}$ expansion the coefficients C_i become functions of the recoil $\omega = \frac{p \cdot p'}{m_c m_b}$.

$$\xi = \frac{m_c}{m_b}, \quad \mathcal{C} = \begin{cases} 1 & ; \Gamma = \gamma^\mu \\ -1 & ; \Gamma = \gamma^\mu \gamma_5 \end{cases}, \quad \tilde{\Gamma} = \begin{cases} 1 & ; \Gamma = \gamma^\mu \\ \gamma_5 & ; \Gamma = \gamma^\mu \gamma_5 \end{cases} \quad (12)$$

The Gordon decomposition of the spinor gives that, for $m_c = m_b$,

$$\bar{u} \gamma^\mu u = \frac{(p + p')^\mu}{2m} \bar{u} u \quad (13)$$

and so the Vector current between degenerate quarks is, of course, not renormalised.

In order to match these currents with Euclidean lattice NRQCD currents we first analytically continue this result to Euclidean space, then apply the Foldy-Wouthuysen expansion of the external spinors [3] to the appropriate order, taking care with the Euclideanised γ -matrices.

A. Analytic Continuation

We define the Euclideanisation as follows. Denoting the Minkowski gamma matrices and four vectors with a caret, $\hat{\gamma}$, so that $\{\hat{\gamma}_\mu, \hat{\gamma}_\nu\} = 2g_{\mu\nu}$, we use the Dirac-Pauli representation:

$$\begin{aligned} \hat{\gamma}^0 &= \hat{\gamma}_0 = \begin{pmatrix} I & 0 \\ 0 & -I \end{pmatrix} \\ \hat{\gamma}^j &= -\hat{\gamma}_j = \begin{pmatrix} 0 & \sigma_j \\ -\sigma_j & 0 \end{pmatrix} \end{aligned} \quad (14)$$

We also define the Euclidean four vectors in terms of the contravariant and covariant Minkowski vectors as:

$$\begin{aligned} x^0 &= x_0 = i\hat{x}^0 = i\hat{x}_0 \\ x^j &= x_j = \hat{x}^j = -\hat{x}_j \end{aligned} \quad (15)$$

We introduce Euclidean γ matrices such that $\{\gamma_\mu, \gamma_\nu\} = 2\delta_{\mu\nu}$

$$\begin{aligned} \gamma^0 &= \gamma_0 = \hat{\gamma}^0 = \hat{\gamma}_0 \\ \gamma^j &= \gamma_j = -i\hat{\gamma}^j = i\hat{\gamma}_j \\ \gamma_5 &= \hat{\gamma}_5 \end{aligned} \quad (16)$$

For consistent notation in Euclidean space, we define Euclidean bilinear currents in terms of the Euclidean γ matrices, so that

$$\begin{aligned} A^0 &= A_0 = \hat{A}^0 = \hat{A}_0 \\ A^j &= A_j = -i\hat{A}^j = i\hat{A}_j \\ V^0 &= V_0 = \hat{V}^0 = \hat{V}_0 \\ V^j &= V_j = -i\hat{V}^j = i\hat{V}_j \end{aligned} \quad (17)$$

Dropping terms in A_k which are subsequently of higher order in $\frac{\bar{p}}{M}$, and suppressing the spinors, this gives us in Euclidean space:

$$\Delta V^0 = \gamma^0 \frac{\alpha_s}{3\pi} \left[-3 \frac{1+\xi}{1-\xi} \log \xi - 4 \right] - 2 \frac{\alpha_s}{3\pi} \quad (18)$$

$$\Delta V^k = \gamma^k \frac{\alpha_s}{3\pi} \left[-3 \frac{1+\xi}{1-\xi} \log \xi - 4 \right] - i \frac{p^k}{m_b} \frac{\alpha_s}{3\pi} \left[-\frac{2}{1-\xi} - \frac{2\xi \log \xi}{(1-\xi)^2} \right] - i \frac{p'^k}{m_c} \frac{\alpha_s}{3\pi} \left[\frac{2\xi}{1-\xi} + \frac{2\xi \log \xi}{(1-\xi)^2} \right] \quad (19)$$

$$\Delta A^0 = \gamma^0 \gamma_5 \frac{\alpha_s}{3\pi} \left[-3 \frac{1+\xi}{1-\xi} \log \xi - 8 \right] + \gamma_5 \frac{\alpha_s}{3\pi} \left[-6 \frac{1+\xi}{1-\xi} - 12 \frac{\xi \log \xi}{(1-\xi)^2} \right] \quad (20)$$

$$\Delta A^k = \gamma^k \gamma_5 \frac{\alpha_s}{3\pi} \left[-3 \frac{1+\xi}{1-\xi} \log \xi - 8 \right]. \quad (21)$$

B. Non-Relativistic Expansion

We now perform the Foldy-Wouthuysen expansion of the external spinors u_h to order $\frac{1}{m}$ in terms of the Euclidean γ matrices to produce two component spinors U_Q :

$$u_h(p) = \left[1 - \frac{i}{2m} \vec{\gamma} \cdot \vec{p} \right] u_Q \quad (22)$$

where

$$u_Q = \begin{bmatrix} U_Q \\ 0 \end{bmatrix} \quad (23)$$

and U_Q is a two component spinor, and m is the pole mass of the quark arising from the on-shell condition (more formally, m is the one loop pole mass whenever it appears at tree level since we are working consistently to order one loop). Inserting this in the results for the continuum renormalisation and keeping terms to order $\frac{1}{M}$ results in the following mixed continuum currents, with the relevant two component spinors suppressed.

$$V^0 = 1_{\text{pauli}} \left[1 + \frac{\alpha_s}{3\pi} \left(-3 \frac{1+\xi}{1-\xi} \log \xi - 6 \right) \right] \quad (24)$$

$$V^k = \left[-i\sigma_k \frac{\sigma \cdot p}{2m_b} - \frac{\sigma \cdot p'}{2m_c} i\sigma_k \right] \left[1 + \frac{\alpha_s}{3\pi} \left(-3 \frac{1+\xi}{1-\xi} \log \xi - 4 \right) \right] \quad (25)$$

$$-i \frac{p_k}{m_b} \frac{\alpha_s}{3\pi} \left[-\frac{2}{1-\xi} - \frac{2\xi \log \xi}{(1-\xi)^2} \right]$$

$$-i \frac{p'_k}{m_c} \frac{\alpha_s}{3\pi} \left[\frac{2\xi}{1-\xi} + \frac{2\xi \log \xi}{(1-\xi)^2} \right]$$

$$A^0 = \left[\frac{\sigma \cdot p}{2m_b} + \frac{\sigma \cdot p'}{2m_c} \right] \left[1 + \frac{\alpha_s}{3\pi} \left(-3 \frac{1+\xi}{1-\xi} \log \xi - 8 \right) \right] \quad (26)$$

$$+ \left[\frac{\sigma \cdot p}{2m_b} - \frac{\sigma \cdot p'}{2m_c} \right] \frac{\alpha_s}{3\pi} \left[-6 \frac{1+\xi}{1-\xi} - 12 \frac{\xi \log \xi}{(1-\xi)^2} \right]$$

$$A_k = -i\sigma_k \left[1 + \frac{\alpha_s}{3\pi} \left(-3 \frac{1+\xi}{1-\xi} \log \xi - 8 \right) \right] \quad (27)$$

We therefore define continuum Euclidean operators Ω_i^J in Table I, to which we wish to match a corresponding set of lattice operators, and use the notation

$$\langle c(p') | J^{\overline{MS}} | b(p) \rangle^{1\text{-loop}} = \sum_{\alpha} Z_{\alpha}^{\overline{MS}} U_{\alpha}^{\dagger} \Omega_{\alpha}^J U_b. \quad (28)$$

The vector current is a conserved current for $m_b = m_c$ and, for this reason, the continuum renormalisation (factor in square brackets in (24)) is unity in the $\xi \rightarrow 1$ limit. The operator corresponding to the temporal component of the vector current, 1_{pauli} , is a conserved current of both the lattice NRQCD and HQET actions, and we shall see that the corresponding lattice renormalisation is also trivial in the $m_b = m_c$ limit.

Unlike the lattice correction, the pure HQET contribution to the vector current renormalisation at zero recoil remains trivial with non-identical quark masses at leading order in $\frac{1}{m_b}$ and $\frac{1}{m_c}$. As a result the above expressions (24) and (27) are the same as the renormalisation at zero recoil for the continuum heavy quark effective theory, commonly referred to as η_V and η_A respectively [4]. This is somewhat fortuitous since it will allow us, in section V, to use the existing result for the BLM scale μ [5,6] for the processes contributing to expressions (24) and (27), with $\mu_V \simeq 0.92\sqrt{m_b m_c}$ and $\mu_A \simeq 0.51\sqrt{m_b m_c}$.

III. LATTICE CALCULATION

A. Lattice action, currents, and Feynman rules

We use the usual Wilson plaquette action [7] defined in terms of the usual SU(3) gauge links $U_{\mu}(x)$, and the tadpole improved [8] $O(\frac{1}{M})$ lattice NRQCD action [9],

$$a\mathcal{L}_{\text{NRQCD}} = \psi^\dagger(x)\psi(x) - \psi^\dagger(x + a\hat{t}) \left(1 - \frac{a\delta H}{2}\right) \left(1 - \frac{aH_0}{2n}\right)^n \frac{U_i^\dagger(x)}{u_0} \left(1 - \frac{aH_0}{2n}\right)^n \left(1 - \frac{a\delta H}{2}\right) \psi(x) \quad (29)$$

where

$$H_0 = -\frac{\Delta^2}{2M_0}, \quad (30)$$

$$\delta H = -c_B \frac{g}{2M_0} \sigma \cdot B, \quad (31)$$

$$\Delta^2 \chi(x) = \frac{1}{u_0} \sum_{i=x,y,z} \left(U_i(x) \chi(x + \hat{i}) + U_i^\dagger(x - \hat{i}) \chi(x - \hat{i}) - 2u_0 \chi(x) \right), \quad (32)$$

and

$$B_i(x) = -\frac{1}{2} \epsilon_{ijk} \left\{ \mathcal{F}_{jk}(x) - \frac{1}{3} \text{Tr} \mathcal{F}_{jk}(x) \right\}, \quad (33)$$

$$\mathcal{F}_{\mu\nu}(x) = \frac{1}{4ag^2} \sum_{\alpha=\pm\mu, \beta=\pm\nu} \frac{[P_{\alpha\beta}(x) - P_{\alpha\beta}^\dagger(x)]}{2i}, \quad (34)$$

$$P_{\alpha\beta}(x) = \frac{1}{u_0^4} U_\alpha(x) U_\beta(x + \hat{\alpha}) U_\alpha^\dagger(x + \hat{\beta}) U_\beta^\dagger(x). \quad (35)$$

In the final results quoted in this paper, u_0 is taken from the plaquette and to one loop order in perturbation theory $u_0^{[1]} = -\frac{\pi}{3}$. However, sufficient information will be presented to allow a reader to change these results for different values of u_0 . To this order in α_s any dynamical quarks present in the simulation do not appear in the perturbation theory. This calculation is therefore applicable to both quenched and dynamical simulations. It is well known how to perform perturbative calculations of the renormalisation of weak currents in NRQCD [10], and the Feynman rules in the Euclidean lattice theory used here are the same as those published by Morningstar and Shigemitsu [10]. This paper completes a programme of work previously discussed at two lattice conferences [11].

Inspection of the continuum currents suggests the basis for the lattice current operators given in Table II. The momentum dependent operators are reproduced on the lattice with gauge covariant derivatives,

$$\nabla_\mu \chi(x) = \frac{1}{2u_0} [U_\mu(x) \chi(x + \hat{\mu}) - U_\mu^\dagger(x - \hat{\mu}) \chi(x - \hat{\mu})] \quad (36)$$

which introduces additional quark gluon vertices that are not present in the continuum theory, as well as a tadpole improvement counter term. For convenience in simulations, we define the lattice operators in terms of the bare mass, M_q . Since we require that the one-loop renormalised kinetic mass in NRQCD matches the one-loop renormalised mass in the relativistic theory³, we must introduce additional Z_m factors for lattice currents wherever the bare mass M_q appears at tree level. The mass ratio ξ appears in the continuum coefficients only at order α_s , and hence the bare ratio $\frac{M_c}{M_b}$ can be used to this order.

We have additional Feynman rules associated with the current operators involving derivatives (and hence gauge links), giving both one and two gluon couplings. The conventions for momenta involved in current insertions of an operator \mathcal{O} both at leading order, and couplings to both 1 and 2 gluons of polarisation j are as given in figure 4.

The Feynman rules associated with the spatial vector and temporal axial currents at the vertex are simply the insertion of the appropriate Pauli structure. The Feynman rules associated with the spatial vector current insertions are as follows

$$\mathcal{O}_1^{V_k}(\text{tree}) = -\frac{i}{2M_b} \sum_j \sin k_j \sigma_k \sigma_j \quad (37)$$

$$\mathcal{O}_1^{V_k}(1 - \text{gluon}) = -\frac{ig}{2M_b} \cos \left[k_j - \frac{1}{2} q_j \right] \sigma_k \sigma_j \quad (38)$$

$$\mathcal{O}_1^{V_k}(2 - \text{gluon}) = \frac{ig^2}{4M_b} \sin \left[k_j - \frac{1}{2} (q_{1j} + q_{2j}) \right] \sigma_k \sigma_j \quad (39)$$

³Lorentz invariance implies that the kinetic and pole masses are consistent in the relativistic theory

$$\mathcal{O}_3^{V_k}(\text{tree}) = -\frac{i}{M_b} \sin k_k \quad (40)$$

$$\mathcal{O}_3^{V_k}(1 - \text{gluon}) = -\frac{ig}{M_b} \cos \left[k_j - \frac{1}{2} q_j \right] \delta_{jk} \quad (41)$$

$$\mathcal{O}_3^{V_k}(2 - \text{gluon}) = \frac{ig^2}{2M_b} \sin \left[k_j - \frac{1}{2} (q_{1j} + q_{2j}) \right] \delta_{jk} \quad (42)$$

where the 1 and 2 gluon couplings are to gluons of polarisation j .

The rules associated with the leftward derivative currents are both the obvious analogues of the above and not in fact required since the diagrams involving the second current may be switched for those of the first current with the masses swapped and momenta reversed, halving the required coding effort. The Feynman rules associated with the first temporal axial lattice current are as follows,

$$\mathcal{O}_1^{A_0}(\text{tree}) = \frac{1}{2M_b} \sum_j \sin k_j \sigma_j \quad (43)$$

$$\mathcal{O}_1^{A_0}(1 - \text{gluon}) = \frac{g}{2M_b} \cos \left(k_j - \frac{1}{2} q_j \right) \sigma_j \quad (44)$$

$$\mathcal{O}_1^{A_0}(2 - \text{gluon}) = \frac{g^2}{4M_b} \sin \left(k_j - \frac{1}{2} (q_{1j} + q_{2j}) \right) \sigma_j \quad (45)$$

while, as above, the rule for the second current is not required.

B. Mixing Matrix

We define the 1-loop mixing matrix of the lattice theory for each of the four currents $J \in \{V_0, V_k, A_0, A_k\}$ as follows:

$$\langle c(p') | \mathcal{O}_\alpha^J | b(p) \rangle^{1\text{-loop}} = \sum_\beta \mathcal{M}_{\alpha\beta}^J U_c^\dagger \Omega_\beta^J U_b, \quad (46)$$

where the range of the summation over β depends on the dimension of the basis for each continuum current. To avoid ambiguity, we shall denote the symbols for lattice Feynman diagrams in bold font to differentiate them from symbols used in the continuum calculation (although the different symbols do not in fact appear in the same equations). For both the temporal vector and spatial axial currents the mixing matrix is rank one, and we have (where J is either V_0 or A_k):

$$\mathcal{M}^J = 1 + \alpha_s \left[\frac{1}{2} \{ \mathbf{Z}_{\psi_c}^{[1]} + \mathbf{Z}_{\psi_b}^{[1]} \} + \mathbf{\Lambda}^{J[1]} \right], \quad (47)$$

$\mathbf{Z}_{\psi}^{[1]}$ gives the relevant leg correction, whose relation to the self energy diagram (Figure 5) is described in appendix A, where we have followed closely the conventions of Morningstar [12]. $\mathbf{\Lambda}^{J[1]}$ corresponds to contributions from the Feynman diagram of Figure 6 where gluon couplings from each of the ∇_t , $\frac{p^2}{2m}$, and $\frac{\sigma \cdot \mathbf{B}}{2m}$ terms in the action are included at each vertex.

For the spatial vector current (and indeed the temporal axial current) the mixing matrix is non-trivial. We denote the vertex correction to each of the lattice currents $\mathcal{O}_\alpha^{V_k}$ from the sum of Feynman diagrams represented in Figures 6 and 8 by $\mathbf{\Lambda}_\alpha^{V_k[1]}$. At one loop the the vertex correction overlaps with each of the corresponding continuum operators, giving rise to the non-trivial mixing problem

$$\mathbf{\Lambda}_\beta^{V_k[1]} = \sum_\alpha \mathbf{\Lambda}_{\alpha\beta}^{V_k[1]} \Omega_\alpha^{V_k}. \quad (48)$$

We resolve the Pauli and momentum structure of $\mathbf{\Lambda}_1^{V_k[1]}$ using the following projections with $j \neq k$, then setting the spatial momenta to zero:

$$\begin{aligned} \mathbf{\Lambda}_{11}^{V_k[1]} &= 2iM_b \sigma_j \sigma_k \frac{\partial}{\partial p_j} \mathbf{\Lambda}_1^{V_k[1]} & \mathbf{\Lambda}_{12}^{V_k[1]} &= 2iM_c \sigma_k \sigma_j \frac{\partial}{\partial p_j} \mathbf{\Lambda}_1^{V_k[1]} \\ \mathbf{\Lambda}_{13}^{V_k[1]} &= iM_b \frac{\partial}{\partial p_k} \mathbf{\Lambda}_1^{V_k[1]} - \frac{1}{2} \mathbf{\Lambda}_{11}^{V_k[1]} & \mathbf{\Lambda}_{14}^{V_k[1]} &= iM_c \frac{\partial}{\partial p_k} \mathbf{\Lambda}_1^{V_k[1]} - \frac{1}{2} \mathbf{\Lambda}_{12}^{V_k[1]}. \end{aligned} \quad (49)$$

We may use the bare lattice mass for convenience in place of the the pole mass in these projections since we are evaluating one-loop coefficients, the difference being $O(\alpha_s^2)$. Mixing matrix elements

$\Lambda_{2\beta}$ are related to $\Lambda_{1\beta}$ by $M_b \leftrightarrow M_c$, and it will be seen later that $\Lambda_{3\beta}$ and $\Lambda_{4\beta}$ are not required for our calculation. Hence we write the contributions to the mixing matrix for the spatial vector current as follows,

$$\mathcal{M}_{\alpha\beta}^{V_k} = \delta_{\alpha\beta} + \alpha_s \left[\begin{aligned} & \frac{1}{2} \{ \mathbf{Z}_{\psi_c}^{[1]} + \mathbf{Z}_{\psi_b}^{[1]} \} \delta_{\alpha\beta} + \{ \mathbf{Z}_{m_b}^{[1]} + \mathbf{Z}_{m_b}^{\text{TI}[1]} \} \{ \delta_{\alpha 1} + \delta_{\alpha 3} \} \delta_{\alpha\beta} \\ & + \{ \mathbf{Z}_{m_c}^{[1]} + \mathbf{Z}_{m_c}^{\text{TI}[1]} \} \{ \delta_{\alpha 2} + \delta_{\alpha 4} \} \delta_{\alpha\beta} + \Lambda_{\alpha\beta}^{V_k[1]} + \Lambda_{\alpha\beta}^{\text{TI}^{V_k}[1]} \end{aligned} \right]. \quad (50)$$

where the the \mathbf{Z}_m factors arise from matching the bare mass in the lattice current to the pole mass in the continuum current to order α_s , and the tadpole improvement counter terms are

$$\mathbf{Z}_m^{\text{TI}[1]} = u_0^{[1]} \left(1 - \frac{3}{2naM_0} \right) \quad (51)$$

$$\Lambda_{\alpha\beta}^{\text{TI}^{V_k}[1]} = -\delta_{\alpha\beta} u_0^{[1]}. \quad (52)$$

Similarly, for the temporal axial current we project the vertex corrections on to the continuum basis using,

$$\Lambda_{11}^{A_0[1]} = 2M_b \sigma_j \frac{\partial}{\partial p_j} \Lambda_1^{A_0[1]}, \quad \Lambda_{12}^{A_0[1]} = 2M_c \sigma_j \frac{\partial}{\partial p_j} \Lambda_1^{A_0[1]}. \quad (53)$$

There is also a tadpole improvement counter term for the temporal axial current,

$$\Lambda_{\alpha\beta}^{\text{TI}^{A_0}[1]} = -\delta_{\alpha\beta} u_0^{[1]}. \quad (54)$$

We write the contributions to the mixing matrix for the temporal axial current as follows,

$$\mathcal{M}_{\alpha\beta}^{A_0} = \delta_{\alpha\beta} + \alpha_s \left[\begin{aligned} & \frac{1}{2} \{ \mathbf{Z}_{\psi_c}^{[1]} + \mathbf{Z}_{\psi_b}^{[1]} \} \delta_{\alpha\beta} + \{ \mathbf{Z}_{m_b}^{[1]} + \mathbf{Z}_{m_b}^{\text{TI}[1]} \} \delta_{\alpha 1} \delta_{\alpha\beta} \\ & + \{ \mathbf{Z}_{m_c}^{[1]} + \mathbf{Z}_{m_c}^{\text{TI}[1]} \} \delta_{\alpha 2} \delta_{\alpha\beta} + \Lambda_{\alpha\beta}^{A_0[1]} + \Lambda_{\alpha\beta}^{\text{TI}^{A_0}[1]} \end{aligned} \right]. \quad (55)$$

The major task in the renormalisation is to calculate the terms in the above mixing matrices numerically using the Feynman rules for the lattice action.

The integrands for each of the Feynman graphs (and their first and second derivatives with respect to both p_i and p'_j where appropriate) were coded in two independent ways in order to verify the correctness of the calculation.

A C++ class was written to encode the Pauli algebra, and wrapped in a Taylor series class giving the first few entries of the (double) expansion in p_j and p'_k . The standard operators were overloaded and standard functions applied the chain rule to their arguments. This enabled the Feynman diagrams to be constructed easily from the Feynman rules, with the Pauli manipulations taken care of by the code. The leading entries in the double Taylor series gave the first few derivatives with respect to p_j and p'_k . Additionally much faster Fortran codes were written with the Pauli manipulations carried out manually, and all derivatives with respect to the external momenta taken by hand. VEGAS [13] was used to evaluate the one loop integrals.

The lattice effective theory is constructed to have the same infra-red physics as the relativistic continuum theory, so that we find the same (cancelling) logarithmic infra-red divergences in the lattice renormalisation in the lattice diagrams as were present in continuum theory. These arise from graphs where a temporally polarised gluon is exchanged via the ∇_t coupling in the action. To handle the infra-red divergent graphs we always perform the integral over k_0 analytically, and then integrate infra-red finite sums of graphs, e.g. $\frac{1}{2} \{ \mathbf{Z}_{\psi_c}^{[1]} + \mathbf{Z}_{\psi_b}^{[1]} \} + \Lambda_{11}^{[1]}$, over the remaining three dimensions corresponding to the spatial components of the loop momentum.

IV. MATCHING AND RESULTS

We wish to form a linear combination of the lattice currents such that they match the continuum currents at one loop. We reconstruct the \overline{MS} continuum currents from the lattice currents as follows,

$$\begin{aligned} \langle c(p') | J^{\overline{MS}} | b(p) \rangle^{1\text{-loop}} &= \sum_{\alpha,\beta} Z_{\alpha}^{\overline{MS}} (\mathcal{M}^J)_{\alpha\beta}^{-1} \langle c(p') | \mathcal{O}_{\beta}^J | b(p) \rangle^{1\text{-loop}} \\ &= \sum_{\beta} [Z_{\beta}^{\text{tree}} + \alpha_s \rho_{\beta}^J] \langle c(p') | \mathcal{O}_{\beta}^J | b(p) \rangle^{1\text{-loop}} \end{aligned} \quad (56)$$

where $Z_{\beta}^{\text{tree}} \in \{0, 1\}$ is the tree level piece of $Z_{\beta}^{\overline{MS}}$

In what follows we shall present results for the ρ_β for each of the currents in turn as a function of both the bare lattice mass $\frac{1}{M_b}$ and the mass ratio $\xi = \frac{M_c}{M_b}$. For reasons of practicality, we make the stabilisation parameters for each quark, n_c and n_b , implicit functions of the mass as indicated in table III.

A. Temporal Vector Current

For the temporal vector current we have

$$V_0^{\overline{MS}} = \{1 + \alpha_s \rho^{V_0}\} \mathcal{O}^{V_0}, \quad (57)$$

$$\rho^{V_0} = B^{V_0} - \frac{1}{2} \{ \mathbf{Z}_{\psi_c}^{[1]} + \mathbf{Z}_{\psi_b}^{[1]} \} - \mathbf{\Lambda}^{V_0[1]}, \quad (58)$$

$$B^{V_0} = \frac{1}{3\pi} \left[-3 \frac{1+\xi}{1-\xi} \log \xi - 6 \right], \quad (59)$$

We plot the renormalisation coefficient ρ^{V_0} in figure 10. In table IV we give the correction as a function of $\frac{1}{M_b}$ for $\xi = 0.1, 0.2, 0.3, 0.4, 0.5$ and 1.0, useful ratios for lattice simulations. Since the lattice current is conserved, the one-loop renormalisation coefficient vanishes, for all M_b in the case $\xi = 1$, as clearly shown by figure 10.

Luke's theorem [14] shows that there is no $O(\frac{1}{M})$ correction to form factors involving the vector current in HQET at zero recoil. Luke's theorem is a non-perturbative observation based upon the symmetries of HQET. The required symmetries are satisfied by Lattice NRQCD, and the theorem should certainly be manifested in the one-loop coefficients at zero-recoil. Demonstrating this is less trivial than in HQET however, since M dependence arises out of terms in the action as well as through current insertions, and we proceed by numerically calculating the M dependence of the lattice NRQCD contribution to the renormalisation. In figure 11 we display the lattice one loop renormalisation $\rho^{V_0} - B^{V_0}$ plotted versus $(\frac{1}{M_c} - \frac{1}{M_b})^2$, for various values of $\xi = \frac{M_c}{M_b}$. This plot shows that the leading correction is linear in $(\frac{1}{M_c} - \frac{1}{M_b})^2$ in the $\frac{1}{M} \rightarrow 0$ region, with a universal slope. This is consistent with the absence of the $\frac{1}{M}$ term, as expected by Luke's theorem applied to lattice NRQCD.

Of course the analogue of Luke's theorem should be held non-perturbatively by lattice NRQCD, and a fit of the dependence of the non-perturbative lattice form factor on $\frac{1}{M_b}$ near the static limit should be made on simulation data to check the consistency with Luke's theorem.

B. Spatial Axial Current

For the spatial axial current,

$$A_k^{\overline{MS}} = \{1 + \alpha_s \rho^{A_k}\} \mathcal{O}^{A_k}, \quad (60)$$

$$\rho^{A_k} = B^{A_k} - \frac{1}{2} \{ \mathbf{Z}_{\psi_c}^{[1]} + \mathbf{Z}_{\psi_b}^{[1]} \} - \mathbf{\Lambda}^{A_k[1]}, \quad (61)$$

$$B^{A_k} = \frac{1}{3\pi} \left[-3 \frac{1+\xi}{1-\xi} \log \xi - 8 \right]. \quad (62)$$

We plot the renormalisation coefficient ρ^{A_k} in figure 12, and give the correction as a function of $\frac{1}{M_b}$ for $\xi = 0.1, 0.2, 0.3, 0.4, 0.5$ and 1.0 in table V.

C. Temporal Axial Current

For the temporal axial current we have

$$A_0^{\overline{MS}} = \{1 + \alpha_s \rho_1^{A_0}\} \mathcal{O}_1^{A_0} + \{1 + \alpha_s \rho_2^{A_0}\} \mathcal{O}_2^{A_0} \quad (63)$$

where

$$\rho_1^{A_0} = B_1^{A_0} - \frac{1}{2} \{ \mathbf{Z}_{\psi_c}^{[1]} + \mathbf{Z}_{\psi_b}^{[1]} \} - \mathbf{\Lambda}_{11}^{A_0[1]} - \mathbf{\Lambda}_{21}^{A_0[1]} - \mathbf{Z}_{m_b}^{[1]} - \mathbf{\Lambda}_{11}^{\text{TI}^{A_0}[1]} - \mathbf{Z}_{m_b}^{\text{TI}[1]} \quad (64)$$

$$\rho_2^{A_0} = B_2^{A_0} - \frac{1}{2} \{ \mathbf{Z}_{\psi_c}^{[1]} + \mathbf{Z}_{\psi_b}^{[1]} \} - \mathbf{\Lambda}_{12}^{A_0[1]} - \mathbf{\Lambda}_{22}^{A_0[1]} - \mathbf{Z}_{m_c}^{[1]} - \mathbf{\Lambda}_{22}^{\text{TI}^{A_0}[1]} - \mathbf{Z}_{m_c}^{\text{TI}[1]} \quad (65)$$

and

$$B_1^{A_0} = \frac{1}{3\pi} \left[-3 \frac{1+\xi}{1-\xi} \log \xi - 8 - 6 \frac{1+\xi}{1-\xi} - 12 \frac{\xi \log \xi}{(1-\xi)^2} \right] \quad (66)$$

$$B_2^{A_0} = \frac{1}{3\pi} \left[-3 \frac{1+\xi}{1-\xi} \log \xi - 8 + 6 \frac{1+\xi}{1-\xi} + 12 \frac{\xi \log \xi}{(1-\xi)^2} \right] \quad (67)$$

We plot the renormalisation coefficients $\rho_1^{A_0}$ and $\rho_2^{A_0}$ in figures 13 and 14. The various contributions to $\rho_1^{A_0}$ for $\xi = 0.3$ are given in table VI allowing the reader to see relatively easily the change that must be applied to obtain the coefficients with a different tadpole improvement prescription, such as the mean link in Landau gauge. The diagonal elements $\mathbf{\Lambda}_{\beta\beta}$ of the mixing matrix both contain infra-red divergences which exactly cancel those of the wavefunction renormalisation, and have associated tadpole improvement counter terms associated with the u_0 factor in the derivative operator. It is, in fact, interesting to observe the tadpole improvement programme in action; there are large cancellations between the $\mathbf{Z}_m^{\text{TI}[1]}$ and $\mathbf{Z}_m^{[1]}$ terms and between the $\mathbf{\Lambda}_{11}^{\text{TI}^{A_0}[1]}$ and the $\frac{1}{2} \{ \mathbf{Z}_{\psi_c}^{[1]} + \mathbf{Z}_{\psi_b}^{[1]} \} + \mathbf{\Lambda}_{11}^{A_0[1]}$ terms. This cancellation is even more manifest when we isolate the tadpole graph contributions within $\mathbf{\Lambda}_{11}^{A_0[1]}$ and $\mathbf{Z}_m^{[1]}$. The two overall correction coefficients are tabulated as a function of $\frac{1}{M_b}$ for $\xi = 0.1, 0.2, 0.3, 0.4, 0.5$ and 1.0 in tables VII and VIII.

D. Spatial Vector Current

For the spatial vector current we obtain

$$V_k^{\overline{MS}} = \{ 1 + \alpha_s \rho_1^{V_k} \} \mathcal{O}_1^{V_k} + \{ 1 + \alpha_s \rho_2^{V_k} \} \mathcal{O}_2^{V_k} + \alpha_s \rho_3^{V_k} \mathcal{O}_3^{V_k} + \alpha_s \rho_4^{V_k} \mathcal{O}_4^{V_k} \quad (68)$$

where

$$\rho_1^{V_k} = B_1^{V_k} - \frac{1}{2} \{ \mathbf{Z}_{\psi_c}^{[1]} + \mathbf{Z}_{\psi_b}^{[1]} \} - \mathbf{\Lambda}_{11}^{V_k[1]} - \mathbf{\Lambda}_{21}^{V_k[1]} - \mathbf{Z}_{m_b}^{[1]} - \mathbf{\Lambda}_{11}^{\text{TI}^{V_k}[1]} - \mathbf{Z}_{m_b}^{\text{TI}[1]} \quad (69)$$

$$\rho_2^{V_k} = B_2^{V_k} - \frac{1}{2} \{ \mathbf{Z}_{\psi_c}^{[1]} + \mathbf{Z}_{\psi_b}^{[1]} \} - \mathbf{\Lambda}_{12}^{V_k[1]} - \mathbf{\Lambda}_{22}^{V_k[1]} - \mathbf{Z}_{m_c}^{[1]} - \mathbf{\Lambda}_{22}^{\text{TI}^{V_k}[1]} - \mathbf{Z}_{m_c}^{\text{TI}[1]} \quad (70)$$

$$\rho_3^{V_k} = B_3^{V_k} - \mathbf{\Lambda}_{13}^{V_k[1]} - \mathbf{\Lambda}_{23}^{V_k[1]} \quad (71)$$

$$\rho_4^{V_k} = B_4^{V_k} - \mathbf{\Lambda}_{14}^{V_k[1]} - \mathbf{\Lambda}_{24}^{V_k[1]} \quad (72)$$

$$(73)$$

and

$$B_1^{V_k} = B_2^{V_k} = \frac{1}{3\pi} \left[-3 \frac{1+\xi}{1-\xi} \log \xi - 4 \right] \quad (74)$$

$$B_3^{V_k} = \frac{1}{3\pi} \left[-\frac{2}{1-\xi} - \frac{2\xi \log \xi}{(1-\xi)^2} \right] \quad (75)$$

$$B_4^{V_k} = \frac{1}{3\pi} \left[\frac{2\xi}{1-\xi} + \frac{2\xi \log \xi}{(1-\xi)^2} \right]. \quad (76)$$

Since the \mathcal{O}_3 and \mathcal{O}_4 do not appear at tree level, we can see that it is in fact unnecessary to calculate $\mathbf{\Lambda}_{3\beta}^{V_k}$ and $\mathbf{\Lambda}_{4\beta}^{V_k}$. We plot the renormalisation coefficients $\rho_1^{V_k} \dots \rho_4^{V_k}$ in figures 15 to 18. The various contributions to $\rho_1^{V_k}$ and $\rho_3^{V_k}$ are given for $\xi = 0.3$ in table IX and table X. The four overall correction coefficients are given as a function of $\frac{1}{M_b}$ for $\xi = 0.1, 0.2, 0.3, 0.4, 0.5$ and 1.0 in tables XI to XIV.

V. RELEVANT MOMENTUM SCALE FOR α_s

In section I we argued that the regularisation scheme correction is dominated by ultra-violet physics and is therefore calculable within perturbation theory. This is addressed in this section by attempting to calculate the appropriate scale for α_s in the correction to V_0 and A_k .

The Lepage-Mackenzie q^* scale [8] for some one-loop process whose Feynman amplitude $A = \int \frac{d^4k}{(2\pi)^4} I(k)$ is defined by

$$\log(aq^*)^2 = \frac{\int \frac{d^4k}{(2\pi)^4} I(k) \log(ak)^2}{\int \frac{d^4k}{(2\pi)^4} I(k)}. \quad (77)$$

When a one-loop expression is made up of two sub-processes, $A = \int \frac{d^4k}{(2\pi)^4} I_A(k)$ and $B = \int \frac{d^4k}{(2\pi)^4} I_B(k)$ we may combine the q^* 's as follows,

$$\log(aq^*)_{A+B}^2 = \frac{\int \frac{d^4k}{(2\pi)^4} I_A(k) \log(ak)^2 + \int \frac{d^4k}{(2\pi)^4} I_B(k) \log(ak)^2}{\int \frac{d^4k}{(2\pi)^4} I_A(k) + \int \frac{d^4k}{(2\pi)^4} I_B(k)} \quad (78)$$

or more conveniently,

$$q_{A+B}^* = [(q_A^*)^A \times (q_B^*)^B]^{\frac{1}{A+B}}. \quad (79)$$

Here we shall calculate the Lepage-Mackenzie q^* from lattice perturbation theory, and then use this rule to combine it with the continuum BLM scales from section II B to obtain an overall scale.

The combination of lattice graphs containing the cancelling IR divergences proved troublesome using 4 dimensional numerical integration, so we used the (non-rigorous) Hernandez and Hill prescription [15] to deal with the k_0 integral, and integrated the remaining spatial momenta numerically.

We present the results for $q_{V_0}^*$ in table XV. The overall scale is reassuringly large, and is dominated by the continuum scale due to the typical relative size of the corrections. We therefore believe that the use of Hernandez and Hill prescription to obtain numerical stability constitutes an irrelevant error in the overall scale. We note that $\alpha_V(q^*) \leq 0.22$ for $q^* \geq 3GeV$, which is the case in a typical simulation regimes for V_0 [16].

We present the results for $q_{A_k}^*$ in table XVI. There is a line (straddled by the bold highlighted data in table XVI) in the $\xi - M_b$ plane where q^* becomes poorly behaved. It can be seen in table XVII that the individual scales $q_{A_k}^{*lat}$ and $q_{A_k}^{*cont}$ are large at this point, but that the overall one-loop correction is near vanishing. The location of this uncontrolled behaviour is not dependent on our use of the Hernandez and Hill prescription, however the details of the behaviour will, of course, be somewhat dependent. The zero in the overall correction introduces a vertical asymptote for $\log(aq^*)^2$, due to the vanishing denominator in (78) and consequently a limit of infinity or zero for q^* depending on the direction of approach. The resultant low scale on one side of the zero in the correction is not considered problematic by the authors, since it is a breakdown of the mean scale interpretation of (77), that occurs whenever the correction is small.⁴

The prescription used to set the scale at which to evaluate α_s in a mixing calculation is considered an open question by the authors, however we remain encouraged by the reliability of the perturbation theory suggested by the scales determined thus far.

VI. SUMMARY

We have shown how to construct the \overline{MS} weak decay currents for $B \rightarrow D^{(*)}$ transitions from operators in the lattice NRQCD effective theory at and around the zero recoil point for a wide range of phenomenologically relevant lattice mass parameters. These constants are of use to both recent [16] and future [18] calculations of the semileptonic decay form factors. The one-loop coefficients typically have modulus ≤ 0.3 in the usual simulation regime. The lattice temporal vector current

⁴As noted by Morningstar [17], the integrand $I_A(k) + I_B(k)$ must be either strictly positive or strictly negative for the mean value theorem to guarantee $0 \leq aq^* \leq 2\pi$. Exact cancellation of the integrals is likely to exacerbate the problem.

is not renormalised in the degenerate quark case (this is not the case for Wilson fermions), with the result that the current correction for physical $\frac{m_c}{m_b}$ ratios is particularly small. For two of the currents we have estimated the Lepage-Mackenzie q^* scales, and find that it is large, giving overall one-loop corrections of order $\leq 5\%$, and suggesting perturbation theory is converging adequately. With further suppression, the next (and higher) order corrections in the operator renormalisation could well be below the expected statistical error of the BaBar data.⁵

VII. ACKNOWLEDGMENTS

We wish to thank Junko Shigemitsu for many useful conversations, and cross checking the mass renormalisation. We made use of unpublished notes by Colin Morningstar for checking our continuum calculation. Peter Boyle is supported by PPARC grant PP/CBA/62. Both Peter Boyle and Christine Davies fondly acknowledge the hospitality of the UCSB, Santa Barbara where some of this work was carried out.

-
- [1] The BaBar Physics Book: Physics at an asymmetric B factory.
By BABAR Collaboration (P.F. Harrison, ed. et al.). SLAC-R-0504, Oct 1998.
 - [2] A. Kronfeld, FERMILAB-CONF-98-393-T, hep-ph/9812288.
L. Lellouch, hep-ph/9912353.
S. Aoki, hep-ph/9912288.
S. Hashimoto, *Nucl. Phys. (Proc Suppl)*, **83-84**, 3, (2000).
 - [3] L. Foldy and S. Wouthuysen *Phys. Rev. D*, **48**, 29 (1950)
 - [4] M. Neubert *Phys. Rept.*, **245**, 259, (1994).
 - [5] S. Brodsky, G.P. Lepage, P. Mackenzie *Phys. Rev. D* **28**, 228, (1983).
 - [6] M. Neubert *Phys. Lett. B*, **341**, 367, (1995).
 - [7] K. Wilson *Phys. Rev. D*, **10**, 2445 (1974).
 - [8] G.P. Lepage and P. Mackenzie *Phys. Rev. D* **48**, 2250, (1993).
 - [9] B. Thacker and P. Lepage, *Phys. Rev. D* **43**, 196, (1991).
P. Lepage et. al. *Phys. Rev. D* **46**, 4052, (1992).
 - [10] C. Morningstar, J. Shigemitsu
Phys. Rev. D, **57**, 6741, (1998).
Phys. Rev. D, **59**, 094504, (1999).
Nucl. Phys. (Proc Suppl), **63**, 341, (1998).
 - [11] P. Boyle and C. Davies, *Nucl. Phys. (Proc Suppl)*, **73**, 378, (1999).
P. Boyle and C. Davies Presented at Lattice 99, Pisa, July 1999
 - [12] C. Morningstar, *Phys. Rev. D* **48**, 2265, (1993).
 - [13] G.P. Lepage *J. Comput. Phys.* **27** 192 (1978).
 - [14] M.E. Luke *Phys. Lett. B* **252**, 447 (1990).
 - [15] O. Hernandez and B. Hill, *Phys. Rev. D*, **50**, 495, (1994)
 - [16] J. Hein Presented at Lattice 99, Pisa, July 1999. hep-lat/9908058.
 - [17] C. Morningstar, *Phys. Rev. D* **50**, 5902, (1994).
 - [18] C. Davies, J. Hein, et al *in preparation*.
 - [19] A. Czarnecki, K. Melnikov *Phys. Rev. Lett.* **78**, 3630, (1997).

APPENDIX A: SELF ENERGY CALCULATION

To one loop the graph topologies shown in figures 5 and 9 contribute to the lattice self energy. The diagrams contain contributions from both the temporally polarised gluon vertex, and from spatially

⁵ Certainly, the two loop renormalisation correction to HQET operators is known to be $O(1\%)$ [19].

polarised gluons via the $\frac{p^2}{2m}$ term and via the $\sigma \cdot B$ term. The lattice self energy must satisfy cubic invariance in the spatial momenta, and we write the first terms of a double taylor series for the self-energy as

$$\Sigma^{\text{lat}}(ap_0, a\vec{p}) = g^2 \left\{ \Omega_0 + \Omega_1 iap_0 + \Omega_2 \frac{p^2 a}{2M_0 a} + \dots \right\} \quad (\text{A1})$$

where clearly,

$$g^2 \Omega_0 = \Sigma(0, 0) \quad (\text{A2})$$

$$g^2 \Omega_1 = -i \frac{\partial}{\partial ap_0} \Sigma(0, 0) \quad (\text{A3})$$

$$g^2 \Omega_2 = aM_0 \frac{1}{a^2} \frac{\partial^2}{\partial p_j^2} \Sigma(0, 0) \quad (\text{A4})$$

$$(\text{A5})$$

to order α then the small $\frac{v^2}{c^2}$ expansion of the heavy quark propagator is

$$G_r^{-1}(p) = G^{-1}(p) - \Sigma(ap_0, a\vec{p}) \quad (\text{A6})$$

$$= ip_0 + \frac{p_0^2}{2} + \frac{p^2}{2M_0} - ip_0 \frac{p^2}{2M_0} - g^2 \Omega_0 - iap_0 g^2 \Omega_1 - \frac{p^2}{2M_0} g^2 \Omega_2 \quad (\text{A7})$$

$$= Z_\psi \left(-ia\bar{p}_0 + \frac{p^2 a^2}{2Z_m^{\text{kin}} M a} + \frac{p_0^2 a^2}{2} \right) \quad (\text{A8})$$

where to order g^2 and $\frac{v^2}{c^2}$ we have,

$$i\bar{p}_0 = ip_0 - g^2 \Omega_0 \quad (\text{A9})$$

$$Z_\psi = 1 - g^2 (\Omega_0 + \Omega_1) \quad (\text{A10})$$

$$Z_m^{\text{kin}} = 1 + g^2 (\Omega_2 - \Omega_1) \quad (\text{A11})$$

The contributions from the tadpole diagram figure 9 to Ω_0 and Ω_1 explicitly cancel in Z_ψ due to the equation of motion of the external spinor. In the Z_m calculation, both the tadpole and normal topologies contribute. In order to compute Z_m it was necessary to code a routine to compute the second derivative of the self energy with respect to one of the external spatial momentum components. This was fairly involved, due to the nature of the lattice Feynman rules. There are cancelling infra-red divergences in both Ω_0 and in Ω_1 , so that the integral over the k_0 was performed analytically and the remaining three dimensions integrated numerically. Our numbers for both the Z_ψ , Δ_E , and Z_m agree within statistical error with those of Morningstar and Shigemitsu [10].

FIG. 1. $\alpha_s \Lambda^{\Gamma^{[1]}}$: Continuum vertex correction to $b \rightarrow c$ scattering diagram via weak current $\Gamma = \gamma_\mu$ or $\Gamma = \gamma_\mu \gamma_5$.

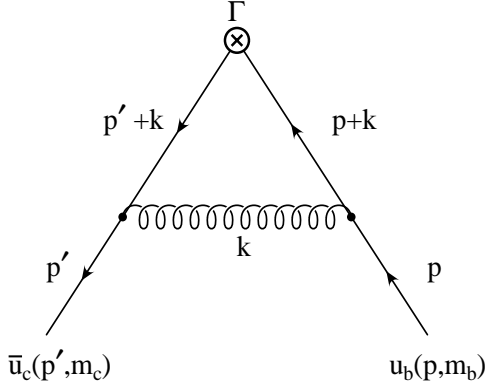


FIG. 2. $\frac{1}{2} \alpha_s \Gamma Z_{\psi_b}^{[1]}$: First leg correction to $b \rightarrow c$ scattering diagram via weak current $\Gamma = \gamma_\mu$ or $\Gamma = \gamma_\mu \gamma_5$.

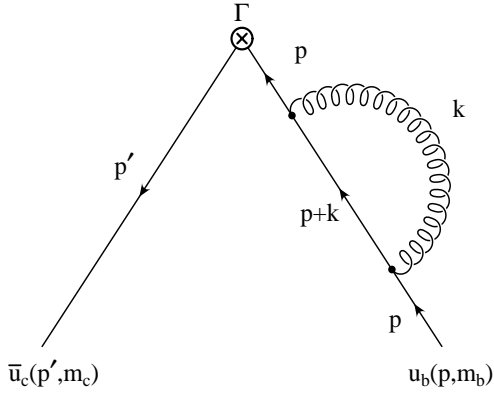


FIG. 3. $\frac{1}{2} \alpha_s \Gamma Z_{\psi_c}^{[1]}$: Second leg correction to $b \rightarrow c$ scattering diagram via weak current $\Gamma = \gamma_\mu$ or $\Gamma = \gamma_\mu \gamma_5$.

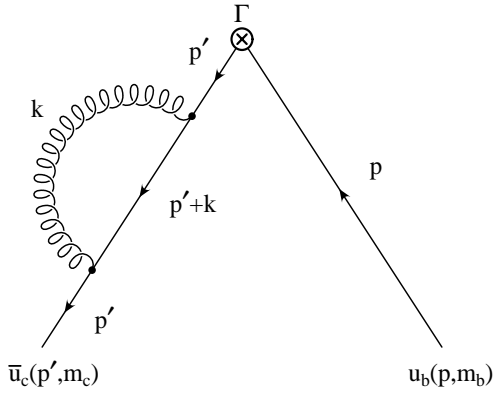


FIG. 4. Feynman rules associated with insertion of a lattice weak current operator to order g^0 , g^1 , and g^2 . The gluon couplings only arise for $\Gamma = V_i$ and $\Gamma = A_0$. Here β runs over the dimension of the lattice operator basis corresponding to the continuum current Γ , as given in Table II.

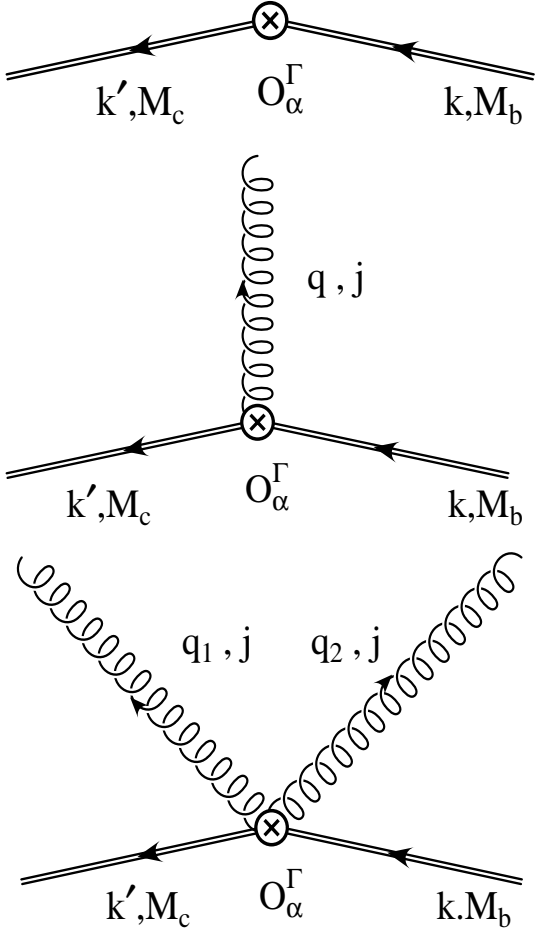


FIG. 5. Regular topology self energy contribution. Contributions arise from a temporally polarised gluon coupling to vertices arising from the ∂_t term in the action, and spatially polarised gluons coupling to vertices arising from the $\frac{p^2}{2m}$ term and the $\frac{\sigma \cdot B}{2m}$ term. For the wavefunction renormalisation the mixed $\frac{\sigma \cdot B}{2m}$ and $\frac{p^2}{2m}$ coupling diagram vanishes at $\vec{p} = 0$, but, since the derivatives do not, the mixed diagrams contribute to the kinetic mass renormalisation.

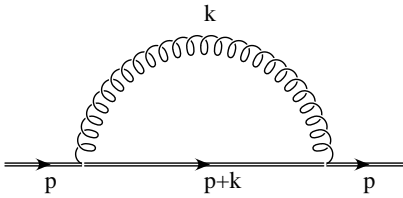


FIG. 6. Regular topology vertex correction.

Temporally polarised gluons couple through the ∂_t term in the action for and spatially polarised gluons through both the $\frac{p^2}{2m}$ and $\frac{\sigma \cdot B}{2m}$ term. Graphs involving mixed $\frac{p^2}{2m}$ and $\frac{\sigma \cdot B}{2m}$ couplings vanish for the temporal vector and spatial axial currents.

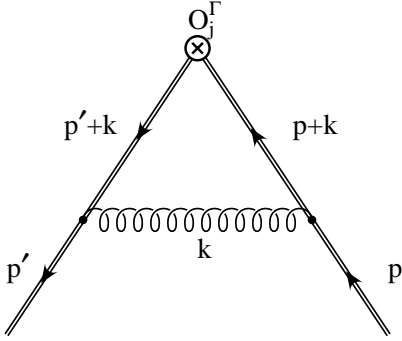


FIG. 7. Diagrams of this topology contribute to both the temporal axial and spatial vector currents. The "tadpole" arises from gauge link in the derivative in the current operators.

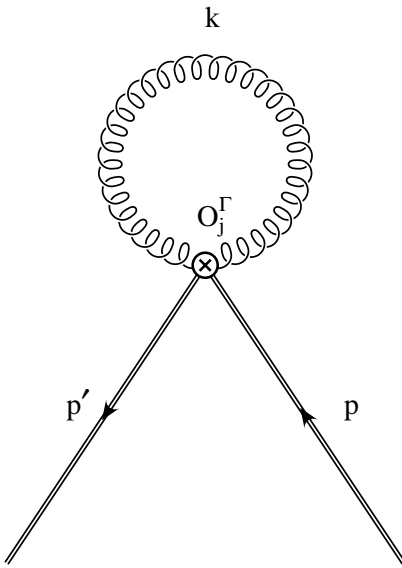
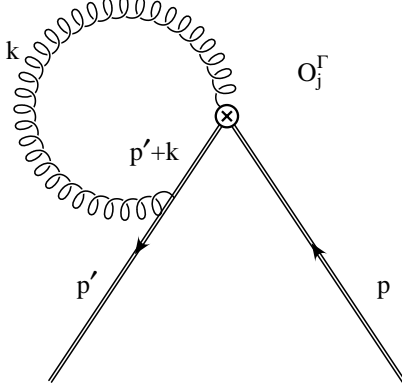


FIG. 8. Diagrams of "left ear" and "right ear" topologies contribute to both the temporal axial and spatial vector currents. The gauge link in the spatial derivative in the current operators creates a coupling to spatially polarised gluons, and the coupling to the leg arises from both the $\frac{p^2}{2m}$ and $\frac{\sigma \cdot B}{2m}$ terms.



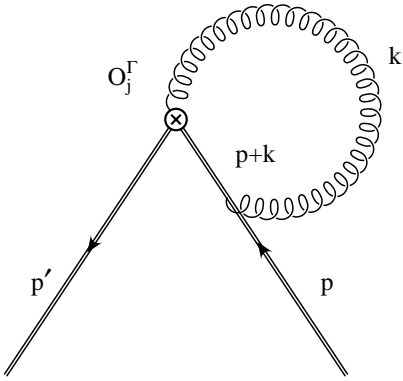


FIG. 9. Tadpole contribution to the self energy. Due to the external equation of motion, this diagram does not in fact contribute to the wavefunction renormalisation, however it does contribute to the kinetic mass renormalisation, through both $\frac{p^2}{2m}$ and $\frac{\sigma \cdot B}{2m}$ two gluon couplings.

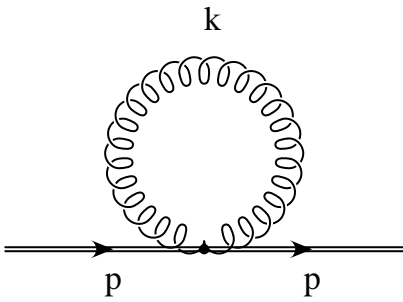


FIG. 10. ρ^{V_0} as a function of ξ and $\frac{1}{M_b}$.

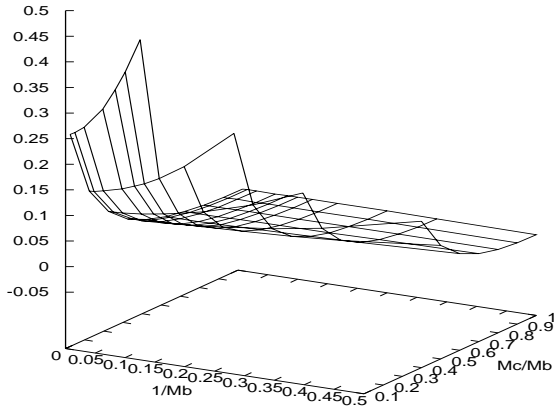


FIG. 11. Pure lattice correction $\rho^{V_0} - B^{V_0}$ as a function of $(\frac{1}{M_c} - \frac{1}{M_b})^2$ for curves $\xi = 0.2 \dots 0.5$ running from top to bottom. The leading correction is linear and universal showing that Luke's theorem is held to one-loop in lattice NRQCD.

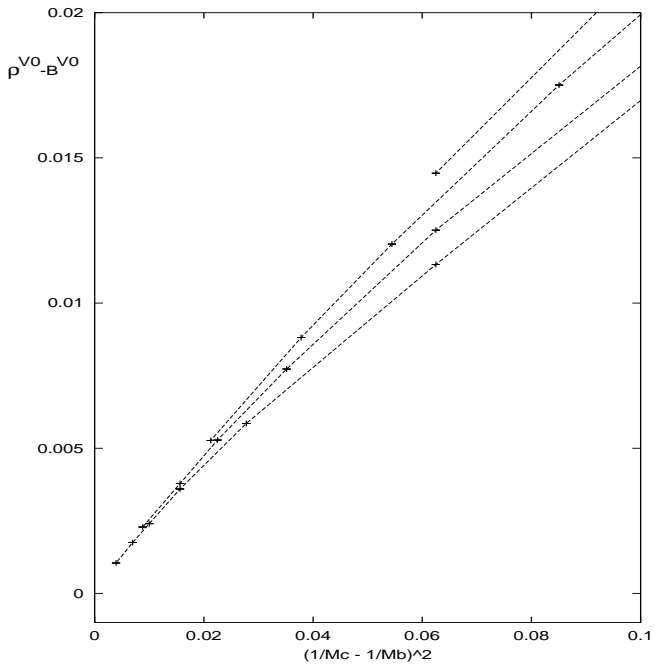


FIG. 12. ρ^{A_k} as a function of ξ and $\frac{1}{M_b}$.

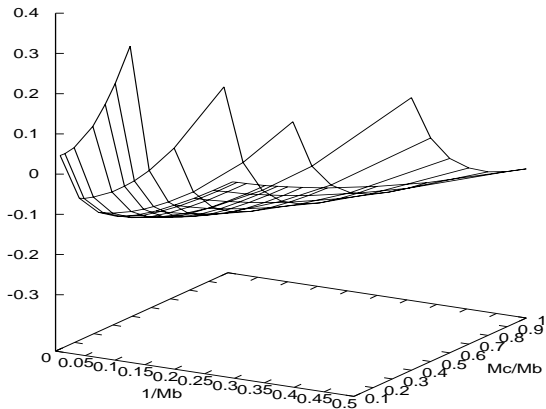


FIG. 13. $\rho_1^{A_0}$ as a function of ξ and $\frac{1}{M_b}$.

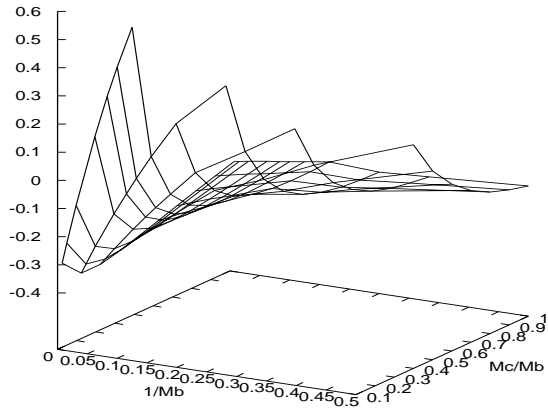


FIG. 14. $\rho_2^{A_0}$ as a function of ξ and $\frac{1}{m_b}$.

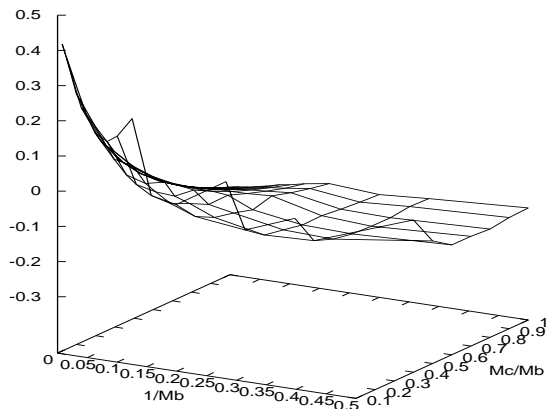


FIG. 15. $\rho_1^{V_k}$ as a function of ξ and $\frac{1}{m_b}$.

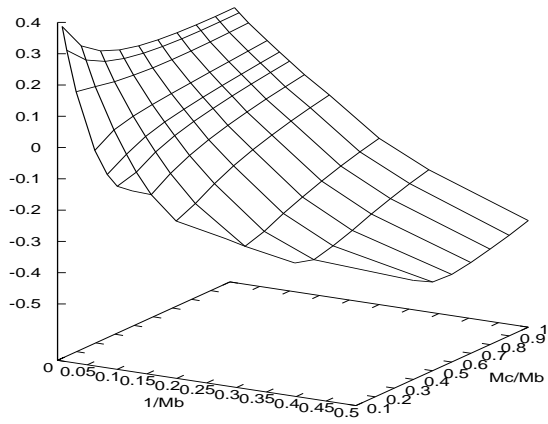


FIG. 16. $\rho_2^{V_k}$ as a function of ξ and $\frac{1}{m_b}$.

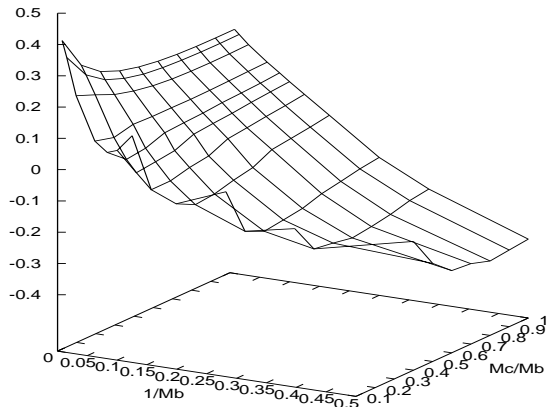


FIG. 17. $\rho_3^{V_k}$ as a function of ξ and $\frac{1}{m_b}$.

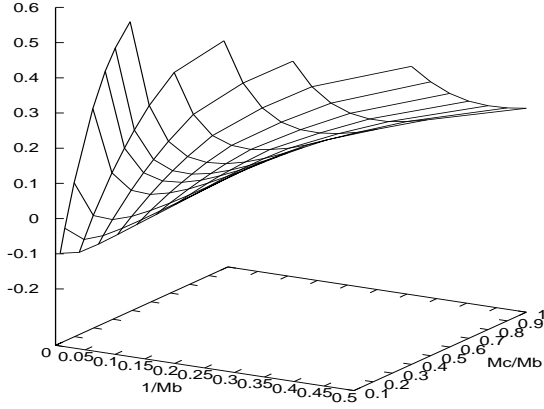


FIG. 18. $\rho_4^{V_k}$ as a function of ξ and $\frac{1}{m_b}$.

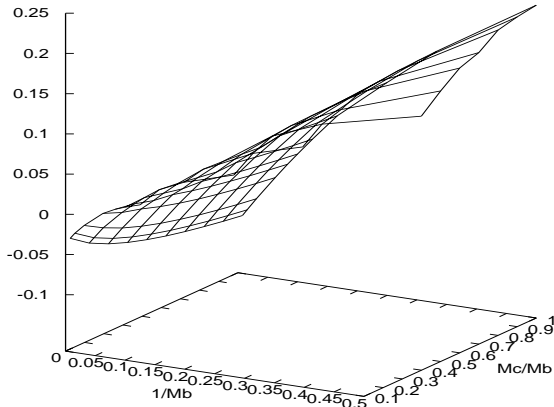


TABLE I. Continuum operators for which we will select corresponding Lattice operators.

V_0	A_k	V_k	A_0
$\Omega_1^{V_0} = 1_{\text{pauli}}$	$\Omega_1^{A_k} = -i\sigma_k$	$\Omega_1^{V_k} = -i\sigma_k \frac{\sigma \cdot p}{2m_b}$ $\Omega_2^{V_k} = -i\frac{\sigma \cdot p}{2m_c} \sigma_k$ $\Omega_3^{V_k} = -i\frac{p_k}{m_b}$ $\Omega_4^{V_k} = -i\frac{p'_k}{m_c}$	$\Omega_1^{A_0} = \frac{\sigma \cdot p}{2m_b}$ $\Omega_2^{A_0} = \frac{\sigma \cdot p'}{2m_c}$

TABLE II. Bases of Lattice Currents to be matched to each of the weak currents.

V_0	A_k	V_k	A_0
$\mathcal{O}_1^{V_0} = \mathbb{1}_{\text{pauli}}$	$\mathcal{O}_1^{A_k} = -i\sigma_k$	$\mathcal{O}_1^{V_k} = -\sigma_k \frac{\vec{\nabla}}{2M_b}$ $\mathcal{O}_2^{V_k} = \frac{\vec{\nabla}}{2M_c} \sigma_k$ $\mathcal{O}_3^{V_k} = -\frac{\vec{\nabla}}{M_b}$ $\mathcal{O}_4^{V_k} = \frac{\vec{\nabla}}{M_c}$	$\mathcal{O}_1^{A_0} = -i \frac{\vec{\nabla}}{2M_b}$ $\mathcal{O}_2^{A_0} = i \frac{\vec{\nabla}}{2M_c}$

TABLE III. Selected stabilisation parameter in different mass regions.

$M \geq 0.8$	$M \geq 1.0$	$M \geq 1.2$	$M \geq 1.6$	$M > 4.0$
n = 5	n=4	n=3	n=2	n=1

 TABLE IV. The one loop piece of the temporal vector current renormalisation for $\xi = 0.1, 0.2, 0.3, 0.4, 0.5$, and 1.0 .

m_b	$\rho^{A_k}(\xi = 0.1)$	$\rho^{A_k}(\xi = 0.2)$	$\rho^{A_k}(\xi = 0.3)$	$\rho^{A_k}(\xi = 0.4)$	$\rho^{A_k}(\xi = 0.5)$	$\rho^{A_k}(\xi = 1.0)$
2.000	-	-	-	0.127146(7)	0.063266(3)	0
3.000	-	-	0.168931(8)	0.084085(3)	0.043936(2)	0
4.000	-	0.28746(1)	0.131438(5)	0.068204(2)	0.0366150(9)	0
6.000	-	0.208433(6)	0.103350(2)	0.0564405(10)	0.0311405(5)	0
8.000	0.46550(2)	0.178367(4)	0.092615(1)	0.0516583(6)	0.0288833(3)	0
10.000	0.39874(1)	0.163900(3)	0.0871368(10)	0.0492116(4)	0.0276885(2)	0
12.000	0.360656(8)	0.155447(2)	0.0839188(7)	0.0477178(3)	0.0270377(1)	0
16.000	0.320742(5)	0.146303(1)	0.0803731(4)	0.0462188(2)	0.02633675(8)	0

 TABLE V. The one loop contribution to the spatial axial current renormalisation for $\xi = 0.1, 0.2, 0.3, 0.4, 0.5$ and 1.0 .

m_b	$\rho^{A_k}(\xi = 0.1)$	$\rho^{A_k}(\xi = 0.2)$	$\rho^{A_k}(\xi = 0.3)$	$\rho^{A_k}(\xi = 0.4)$	$\rho^{A_k}(\xi = 0.5)$	$\rho^{A_k}(\xi = 1.0)$
2.000	-	-	-	0.23875(1)	0.117205(8)	-0.066846(4)
3.000	-	-	0.161977(8)	0.031141(5)	-0.036802(4)	-0.140394(2)
4.000	-	0.251373(9)	0.042554(5)	-0.048200(3)	-0.096478(2)	-0.169133(1)
6.000	-	0.081220(4)	-0.049163(2)	-0.109181(2)	-0.142730(1)	-0.1917372(5)
8.000	0.346311(8)	0.016752(3)	-0.083899(1)	-0.1327985(9)	-0.1605718(7)	-0.2001877(3)
10.000	0.248523(5)	-0.014434(2)	-0.1012549(9)	-0.1445488(6)	-0.1695061(4)	-0.2043054(2)
12.000	0.192853(4)	-0.032424(1)	-0.1112436(7)	-0.1513905(4)	-0.1744741(3)	-0.2066181(1)
16.000	0.134707(2)	-0.0515471(7)	-0.1218945(4)	-0.1583394(3)	-0.1796509(2)	-0.20898845(8)

 TABLE VI. Contributions to the temporal axial current renormalisation for $\xi = 0.3$.

m_b	n_b	m_c	n_c	$\frac{1}{2}\{Z_{\psi_c} + Z_{\psi_b}\} + \Lambda_{11}^{A_0}$	$\Lambda_{21}^{A_0}$	B_1	Z_{m_b}	$Z_{m_b}^{\text{TI}}$	$\Lambda_{11}^{A_0 \text{ TI}}$	ρ_1
3.0	2	0.9	5	-1.3382	-0.6789	-0.3809	1.1458	-0.7854	1.0472	0.2286
4.0	2	1.2	3	-1.2009	-0.5833	-0.3809	1.0861	-0.8508	1.0472	0.1209
6.0	1	1.8	2	-1.0786	-0.4599	-0.3809	0.8770	-0.7854	1.0472	0.0189
8.0	1	2.4	2	-1.0188	-0.3635	-0.3809	0.8761	-0.8508	1.0472	-0.0710
10.0	1	3.0	2	-0.9846	-0.3017	-0.3809	0.8749	-0.8901	1.0472	-0.1266
12.0	1	3.6	2	-0.9623	-0.2574	-0.3809	0.8733	-0.9163	1.0472	-0.1654
16.0	1	4.8	1	-0.9355	-0.1990	-0.3809	0.8708	-0.9490	1.0472	-0.2153
32.0	1	9.6	1	-0.8989	-0.1040	-0.3809	0.8673	-0.9981	1.0472	-0.2944
64.0	1	19.2	1	-0.8806	-0.0534	-0.3809	0.8649	-1.0227	1.0472	-0.3363
128.0	1	38.4	1	-0.8724	-0.0270	-0.3809	0.8636	-1.0349	1.0472	-0.3574

TABLE VII. $\rho_1^{A_0}$ contribution to the temporal axial current renormalisation.

m_b	$\rho_1^{A_0}(\xi = 0.1)$	$\rho_1^{A_0}(\xi = 0.2)$	$\rho_1^{A_0}(\xi = 0.3)$	$\rho_1^{A_0}(\xi = 0.4)$	$\rho_1^{A_0}(\xi = 0.5)$	$\rho_1^{A_0}(\xi = 1.0)$
2.000	-	-	-	0.195(3)	0.070(3)	-0.138(3)
3.000	-	-	0.229(3)	0.068(3)	-0.025(2)	-0.159(2)
4.000	-	0.385(3)	0.121(2)	-0.009(2)	-0.082(2)	-0.169(2)
6.000	-	0.224(2)	0.019(2)	-0.075(2)	-0.126(2)	-0.159(2)
8.000	0.584(2)	0.094(2)	-0.071(2)	-0.141(2)	-0.173(2)	-0.172(1)
10.000	0.435(2)	0.008(2)	-0.127(1)	-0.181(1)	-0.203(1)	-0.180(1)
12.000	0.326(2)	-0.052(1)	-0.165(1)	-0.208(1)	-0.223(1)	-0.185(1)
16.000	0.175(2)	-0.130(1)	-0.215(1)	-0.243(1)	-0.247(1)	-0.190(1)

 TABLE VIII. $\rho_2^{A_0}$ contribution to the temporal axial current renormalisation.

m_b	$\rho_2^{A_0}(\xi = 0.1)$	$\rho_2^{A_0}(\xi = 0.2)$	$\rho_2^{A_0}(\xi = 0.3)$	$\rho_2^{A_0}(\xi = 0.4)$	$\rho_2^{A_0}(\xi = 0.5)$	$\rho_2^{A_0}(\xi = 1.0)$
2.000	-	-	-	-0.027(5)	-0.112(4)	-0.142(3)
3.000	-	-	-0.041(5)	-0.129(4)	-0.149(3)	-0.158(2)
4.000	-	0.067(5)	-0.095(4)	-0.134(3)	-0.145(3)	-0.168(2)
6.000	-	-0.020(4)	-0.079(3)	-0.106(3)	-0.118(2)	-0.158(2)
8.000	0.239(5)	-0.005(3)	-0.052(3)	-0.077(2)	-0.104(2)	-0.170(2)
10.000	0.182(4)	0.020(3)	-0.025(2)	-0.063(2)	-0.070(2)	-0.179(1)
12.000	0.162(4)	0.043(3)	-0.006(2)	-0.027(2)	-0.066(2)	-0.183(1)
16.000	0.182(3)	0.083(2)	0.038(2)	-0.016(2)	-0.060(2)	-0.192(1)

 TABLE IX. Various contributions to the $\rho_1^{V_k}$ spatial vector current renormalisation for $\xi = 0.3$.

m_b	n_b	m_c	n_c	$\frac{1}{2}\{Z_{\psi_c} + Z_{\psi_b}\} + \Lambda_{11}^{V_k}$	$\Lambda_{21}^{V_k}$	B_1	Z_{m_b}	$Z_{m_b}^{\text{TI}}$	$\Lambda_{11}^{V_k \text{ TI}}$	ρ_1
3.0	2	0.9	5	-1.4361	0.6402	0.2873	1.1496	-0.7854	1.0472	-0.3281
4.0	2	1.2	3	-1.2605	0.5574	0.2873	1.0932	-0.8508	1.0472	-0.2991
6.0	1	1.8	2	-1.1096	0.4418	0.2873	0.8795	-0.7854	1.0472	-0.1862
8.0	1	2.4	2	-1.0372	0.3520	0.2873	0.8786	-0.8508	1.0472	-0.1024
10.0	1	3.0	2	-0.9971	0.2933	0.2873	0.8748	-0.8901	1.0472	-0.0407
12.0	1	3.6	2	-0.9719	0.2510	0.2873	0.8734	-0.9163	1.0472	0.0039
16.0	1	4.8	1	-0.9406	0.1951	0.2873	0.8720	-0.9490	1.0472	0.0626
32.0	1	9.6	1	-0.8983	0.1031	0.2873	0.8696	-0.9981	1.0472	0.1638
64.0	1	19.2	1	-0.8806	0.0527	0.2873	0.8663	-1.0227	1.0472	0.2243
128.0	1	38.4	1	-0.8721	0.0268	0.2873	0.8649	-1.0349	1.0472	0.2555

 TABLE X. Various contributions to the $\rho_3^{V_k}$ spatial vector current renormalisation for $\xi = 0.3$.

m_b	n_b	m_c	n_c	$\Lambda_{13}^{V_k}$	$\Lambda_{23}^{V_k}$	B_3	ρ_3
3.0	2	0.9	5	-0.0091	-0.6212	-0.1467	0.4836
4.0	2	1.2	3	-0.0052	-0.5416	-0.1467	0.4001
6.0	1	1.8	2	-0.0030	-0.4333	-0.1467	0.2896
8.0	1	2.4	2	-0.0017	-0.3472	-0.1467	0.2022
10.0	1	3.0	2	-0.0010	-0.2897	-0.1467	0.1439
12.0	1	3.6	2	-0.0007	-0.2483	-0.1467	0.1022
16.0	1	4.8	1	-0.0004	-0.1933	-0.1467	0.0470
32.0	1	9.6	1	-0.0001	-0.1024	-0.1467	-0.0442
64.0	1	19.2	1	-0.0000	-0.0527	-0.1467	-0.0940
128.0	1	38.4	1	-0.0000	-0.0267	-0.1467	-0.1200

TABLE XI. $\rho_1^{V_k}$ contribution to spatial vector current renormalisation.

m_b	$\rho_1^{V_k}(\xi = 0.1)$	$\rho_1^{V_k}(\xi = 0.2)$	$\rho_1^{V_k}(\xi = 0.3)$	$\rho_1^{V_k}(\xi = 0.4)$	$\rho_1^{V_k}(\xi = 0.5)$	$\rho_1^{V_k}(\xi = 1.0)$
2.000	-	-	-	-0.364(3)	-0.396(3)	-0.339(3)
3.000	-	-	-0.328(3)	-0.346(2)	-0.329(2)	-0.225(2)
4.000	-	-0.247(3)	-0.299(2)	-0.279(2)	-0.250(2)	-0.149(2)
6.000	-	-0.214(2)	-0.186(2)	-0.151(2)	-0.121(2)	-0.034(2)
8.000	-0.102(2)	-0.142(2)	-0.102(2)	-0.073(2)	-0.050(2)	0.018(2)
10.000	-0.095(2)	-0.077(2)	-0.041(2)	-0.016(1)	0.000(1)	0.055(1)
12.000	-0.062(2)	-0.025(2)	0.004(1)	0.022(1)	0.035(1)	0.079(1)
16.000	0.009(2)	0.047(1)	0.063(1)	0.072(1)	0.079(1)	0.110(1)

 TABLE XII. $\rho_2^{V_k}$ contribution to spatial vector current renormalisation.

m_b	$\rho_2^{V_k}(\xi = 0.1)$	$\rho_2^{V_k}(\xi = 0.2)$	$\rho_2^{V_k}(\xi = 0.3)$	$\rho_2^{V_k}(\xi = 0.4)$	$\rho_2^{V_k}(\xi = 0.5)$	$\rho_2^{V_k}(\xi = 1.0)$
2.000	-	-	-	-0.168(5)	-0.266(4)	-0.328(3)
3.000	-	-	-0.148(4)	-0.240(4)	-0.250(3)	-0.216(2)
4.000	-	-0.026(5)	-0.181(4)	-0.208(3)	-0.200(3)	-0.139(2)
6.000	-	-0.089(4)	-0.119(3)	-0.113(2)	-0.097(2)	-0.029(2)
8.000	0.145(5)	-0.056(3)	-0.055(2)	-0.040(2)	-0.031(2)	0.026(1)
10.000	0.090(4)	-0.009(3)	-0.002(2)	0.006(2)	0.031(2)	0.060(1)
12.000	0.079(4)	0.029(2)	0.037(2)	0.058(2)	0.063(2)	0.083(1)
16.000	0.109(3)	0.093(2)	0.107(2)	0.105(2)	0.104(2)	0.111(1)

 TABLE XIII. $\rho_3^{V_k}$ contribution to spatial vector current renormalisation.

m_b	$\rho_3^{V_k}(\xi = 0.1)$	$\rho_3^{V_k}(\xi = 0.2)$	$\rho_3^{V_k}(\xi = 0.3)$	$\rho_3^{V_k}(\xi = 0.4)$	$\rho_3^{V_k}(\xi = 0.5)$	$\rho_3^{V_k}(\xi = 1.0)$
2.000	-	-	-	0.487(2)	0.418(2)	0.2193(9)
3.000	-	-	0.484(2)	0.386(1)	0.315(1)	0.1435(7)
4.000	-	0.545(2)	0.400(1)	0.305(1)	0.2393(9)	0.0955(5)
6.000	-	0.433(1)	0.290(1)	0.2045(8)	0.1519(7)	0.0441(4)
8.000	0.592(2)	0.329(1)	0.2022(8)	0.1340(7)	0.0927(6)	0.0105(3)
10.000	0.510(1)	0.2526(9)	0.1439(7)	0.0875(6)	0.0529(5)	-0.0109(2)
12.000	0.440(1)	0.1970(8)	0.1022(6)	0.0540(5)	0.0255(4)	-0.0256(2)
16.000	0.329(1)	0.1214(6)	0.0470(4)	0.0104(4)	-0.0102(3)	-0.0446(2)

 TABLE XIV. $\rho_4^{V_k}$ contribution to spatial vector current renormalisation.

m_b	$\rho_4^{V_k}(\xi = 0.1)$	$\rho_4^{V_k}(\xi = 0.2)$	$\rho_4^{V_k}(\xi = 0.3)$	$\rho_4^{V_k}(\xi = 0.4)$	$\rho_4^{V_k}(\xi = 0.5)$	$\rho_4^{V_k}(\xi = 1.0)$
2.000	-	-	-	0.1458(7)	0.1664(8)	0.2188(9)
3.000	-	-	0.0997(5)	0.1171(6)	0.1244(6)	0.1429(7)
4.000	-	0.0661(4)	0.0823(4)	0.0930(5)	0.0952(5)	0.0946(5)
6.000	-	0.0478(3)	0.0532(3)	0.0517(3)	0.0501(4)	0.0438(4)
8.000	0.0259(2)	0.0339(3)	0.0310(3)	0.0271(3)	0.0234(3)	0.0100(3)
10.000	0.0202(2)	0.0212(2)	0.0159(2)	0.0106(2)	0.0089(2)	-0.0112(2)
12.000	0.0157(2)	0.0116(2)	0.0048(2)	0.0014(2)	-0.0047(2)	-0.0258(2)
16.000	0.0081(1)	-0.0015(1)	-0.0080(2)	-0.0158(2)	-0.0224(2)	-0.0448(2)

TABLE XV. The overall Lepage-Mackenzie scale $aq_{V_0}^*$ for the current V_0 as a function of M_b and ξ .

m_b	$aq_{V_0}^*(\xi = 0.1)$	$aq_{V_0}^*(\xi = 0.2)$	$aq_{V_0}^*(\xi = 0.3)$	$aq_{V_0}^*(\xi = 0.4)$	$aq_{V_0}^*(\xi = 0.5)$	$aq_{V_0}^*(\xi = 1.0)$
2.000	-	-	-	1.6	1.6	∞
3.000	-	-	1.7	1.7	1.8	∞
4.000	-	1.7	1.8	2.0	2.2	∞
6.000	-	2.1	2.4	2.8	3.1	∞
8.000	2.0	2.6	3.2	3.8	4.3	∞
10.000	2.3	3.3	4.1	4.9	5.5	∞
12.000	2.7	4.0	5.1	6.0	6.8	∞
16.000	3.6	5.5	7.0	8.3	9.5	∞

TABLE XVI. The overall Lepage-Mackenzie scale $aq_{A_k}^*$ for the current A_k as a function of M_b and ξ .

m_b	$aq_{A_k}^*(\xi = 0.1)$	$aq_{A_k}^*(\xi = 0.2)$	$aq_{A_k}^*(\xi = 0.3)$	$aq_{A_k}^*(\xi = 0.4)$	$aq_{A_k}^*(\xi = 0.5)$	$aq_{A_k}^*(\xi = 1.0)$
2.000	-	-	-	3.6	6.8	0.4
3.000	-	-	3.1	27.9	0.2	1.6
4.000	-	2.1	5.1	0.8	1.4	2.2
6.000	-	1.8	2.1	2.3	2.5	3.4
8.000	1.6	0.5	3.1	3.1	3.3	4.4
10.000	1.6	24.0	3.7	3.8	4.1	5.5
12.000	1.6	8.3	4.2	4.4	4.8	6.5
16.000	1.7	6.8	5.3	5.7	6.2	8.5

TABLE XVII. Here we show the constituent lattice and continuum pieces of $aq_{A_k}^*$ in the regions noted in bold in table XVI. It can be seen that the cancellation between the lattice and continuum one-loop correction is resulting in unstable behaviour for the overall scale.

m_b	m_c	aq_{LAT}^*	aq_{cont}^*	Z_{LAT}	Z_{cont}	aq_{all}^*
2.0	1.0	1.73	0.74	0.3039	-0.1869	6.8
2.0	2.0	1.63	1.04	0.1453	-0.2122	0.4
3.0	1.2	1.66	0.99	0.1992	-0.1683	27.9
3.0	1.5	1.62	1.10	0.1501	-0.1869	0.2
4.0	1.2	1.63	1.14	0.1795	-0.1371	5.1
4.0	1.6	1.58	1.32	0.1200	-0.1683	0.8
6.0	1.8	1.50	1.71	0.0878	-0.1371	2.1
8.0	1.6	1.48	1.86	0.0971	-0.0804	0.5
10.0	2.0	1.40	2.33	0.0660	-0.0804	24.0